ORIGINAL ARTICLE

Molecular weight-dependent physisorption of non-charged poly(9,9-dioctylfluorene) onto the neutral surface of cuboidal γ-alumina in toluene

Kazuki Yamazaki[1] · Ayako Nakao[1] · Nozomu Suzuki[2] · Michiya Fujiki [1]

Abstract

To understand how polymers physisorb onto solid surfaces, we investigated the physisorption behavior of non-charged, semiflexible poly(9,9-dioctylfluorene) (**PF8**) with three different number-average degrees of polymerization (DP_n) as photoluminescent and chromophoric probes onto cuboidal γ-alumina in toluene at 5, 25, and 50 °C. **PF8** revealed noticeable DP_n and temperature dependencies in its physisorption behaviors. Molecular mechanics (MM)/molecular dynamics (MD) simulations [consistent valence force field (CVFF)] and Møller–Plesset second-order perturbation theory (MP2) with 6-31 G (d,p) calculations suggested that the **PF8** in toluene has multiple interactions from CH/π to C–H/O interactions on the (110) surface of γ-alumina. The competition between multiple intermolecular CH/π and C–H/O interactions was crucial for the spontaneous physisorption of **PF8** to occur in the presence of a solvent quantity of toluene. Calculations by time-dependent density functional theory (TD-DFT) with Becke three parameter Lee-Yang-Par (B3LYP) method and 6–31 G(d,p) basis set of a model fluorene 9-mer indicated that the π–π* absorption wavelength largely depends on the regularity of the dihedral angles between fluorene rings, while the intensity and spectral width of the π–π* absorption band are largely influenced by the regularity of the dihedral angles. Solution-phase physisorption systems are a result of the inherent nature of several competitive weak intermolecular interactions coexisting among the polymers, surface, and solvents.

Introduction

Physisorption is a ubiquitous phenomena at gas-liquid, liquid-solid, and gas-solid interfaces [1–4]. Historically, physisorption phenomena of small molecules at gas-solid and liquid-solid interfaces are understood well [5, 6]. Physisorbed flexible polymers at surfaces are postulated to adopt the loop-train-tail structure [7]. Physisorption is a consequence of several non-covalent interactions [3, 4] and is assumed to be the initial process of covalent bonds that originate from chemisorption. An organosilane coupling reagent and end-functionalized polymer enable the modification of the desired functional surface of ceramics [8–12]. However, a deeper understanding of the physisorption behavior of chain-like polymers at liquid-solid interfaces remains an unresolved issue. This difficulty arises from the large conformational freedom of the main-chain/side-chain of polymers, as well as the nature of the surrounding solvent molecules. Thus far, the investigation of physisorption phenomena has focused on non-chromophoric and/or non-luminophoric polymers, such as polystyrene derivatives and polyethylene glycol, with the goal of using them for several potent applications [1–11]. Nevertheless, liquid-phase physisorption of chain-like polymers is beneficial for the hybridization of polymers with inorganics, such as metal oxides, chalcogenides, and noble metals, when inexpensive functional source materials are employed at ambient temperatures [12, 13] in addition to various sophisticated approaches used thus far to modify surfaces [14–29].

In 2007, Tavenner et al. investigated how fluorobenzene and hexafluorobenzene (C_6F_6) can physisorb onto the polar HO-Al surface of alumina by means of solid-state ^{19}F-NMR

✉ Michiya Fujiki
   fujikim@ms.naist.jp

1   Graduate School of Materials Science, Nara Institute of Science and Technology, 8916-5, Takayama, Ikoma Nara 630-0192, Japan

2   Department of Chemistry, College of Science, Rikkyo University, 3-34-1 Nishi-Ikebukuro, Toshima, Tokyo 171-8501, Japan

Fig. 1 Chemical structure of **PF8** (top, left) and proposed intramolecular CH/π interactions between four H atoms at the β-carbon atoms of the *n*-octyl groups and four carbon atoms at the *ipso*-carbons of the two fluorene rings (top, right). Chemical structures of **F8** (bottom, left) and **F1-2/F1-9** (bottom, right) for the MP2 (6-31 G(d,p)) and TD-DFT (B3LYP/6-31 G(d,p)) calculations

F8 for MP2 (6-31G(d,p)) calculation

F1-2 : *n* = 2 for MP2 (6-31G(d,p)) calculation

F1-9: *n* = 9 for DFT/TD-DFT (B3LYP / 6-31G(d,p)) calculation
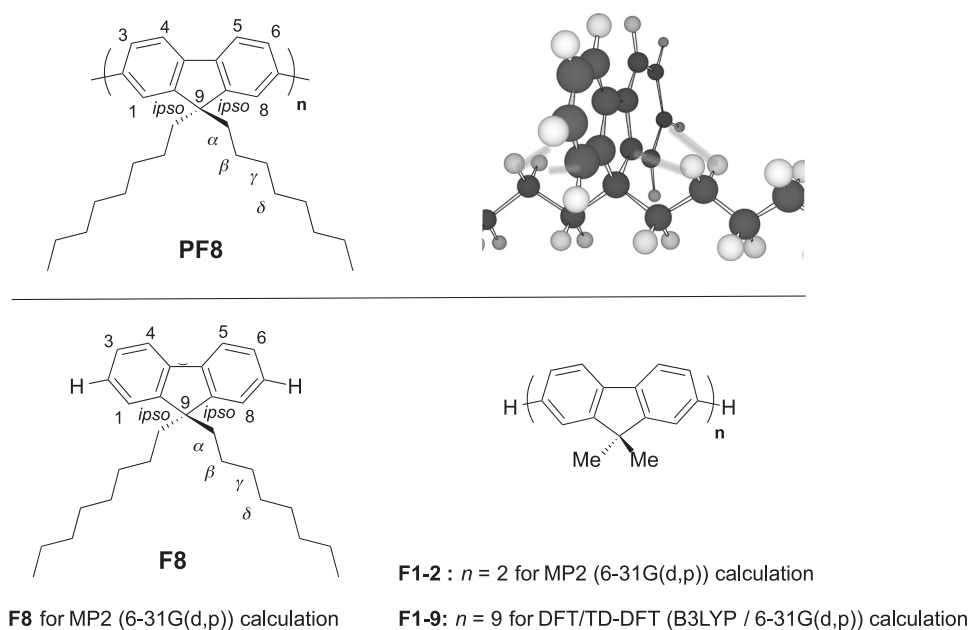
and FT-IR spectroscopy. A noticeable reorientation of C_6F_6 from face-on to edge-on geometry at the HO-Al surface occurred when the surface coverage increased [30]. Recently, Pietropaola et al. indicated the importance of interactions between semiflexible poly(9,9-*n*-dioctyl-fluorene) (**PF8**) and amorphous silica in the origin of the nonhelical-to-helical phase transition at the quartz surface by means of well-tempered meta-dynamic molecular dynamics (MD) simulations [31]. Zhang, Gomez, and Milner theoretically discussed the inherent nature of semi-flexible polymer chains associated with the persistence length (*q*) at an impenetrable surface, such as ceramics and metals, because the physisorption behavior of semiflexible polymers is different from that of flexible polymers. Their MD simulation based on a bead-spring model predicts that semiflexible polymers will spontaneously parallelly align in a nematic-like phase at the surface [32].

Non-charged **PF8** in solution and solid states has been established to be susceptible to the dihedral angles among fluorene rings associated with higher-order structures, known as α-phase, β-phase, and other phases [33–40]. The longest π–π* transition at ≈435 nm is characteristic of the β-phase due to the well-ordered packing state of **PF8** main chains, while the π–π* transitions at 330–390 nm, which largely blueshifted by 30–50 nm, are from the α-, α'-, liquid crystalline, and amorphous phases.

These inherent nature of **PF8** facilitates us to investigate the relationship between the physisorption behaviors and higher-order structures of **PF8** as a realistic semiflexible polymer model. Moreover, **PF8** has a unique chemical structure that can avoid aggregation-caused quenching (ACQ) from which many π-conjugated compounds suffer

[41]. The key geometry for the non-ACQ behavior is that the long axis of the side chain is oriented perpendicular to the plane of the fluorene ring, and the conformation of the two alkyl side chains at the 9,9 positions is stabilized by intramolecular C–*H*/π interactions, as illustrated in Fig. 1 (top right) [42]. This intramolecular C–*H*/π interaction efficiently prevents π–π stacking, leading to the non-ACQ behavior. Recently, this idea was verified by a single-crystal structural analysis of several 9,9-dialkylfluorene molecules, as well as variable temperature ^{1}H-NMR measurements in 1,1,2,2-tetrahloroethane-d_2[43].

In two previous papers, we spectroscopically visualized the physisorption behavior of polymers at a liquid-solid interface using non-charged, photoluminescent **PF8** with a smaller DP_n of 43 and a wider polydispersity index (*PDI*) of ≈4.5 as a model of a stiff, chainlike adsorbate and 0.5 μm-size spherical silica particles as a non-charged, adsorbent *amorphous surface*[44, 45]. We expected the efficient production of a higher fraction of the β-phase by solution-phase epitaxy growth at the crystalline surface of γ-alumina even in *dilute/semi-dilute* conditions, but a dominant facet was not characterized. When the molecular weight of **PF8** increased, we found a noticeable increase in the β-phase and rapid physisorption within one hour in several common organic solvents [45]. A detailed DP_n dependency of the physisorption behavior at a crystalline solid surface, how-ever, was not reported.

In this paper, we investigated the physisorption behavior of **PF8** onto *crystalline*, cuboidal γ-alumina (90–120 m^2 g^{-1}) in toluene at 5, 25, and 50 °C. **PF8** revealed noticeable DP_n and temperature dependencies of its physisorption beha-viors. Molecular mechanics (MM)/molecular dynamics

(MD) simulations with consistent valence force field (CVFF) [34, 46] and Møller–Plesset second-order perturbation theory (MP2) with 6-31 G(d,p) basis set [47, 48] calculations suggested that **PF8** swaps multiple interactions, e.g., CH/π interactions [49–51] to C–H/O interactions [52–54], at the (110) surface of γ-alumina in toluene. The competition among multiple intermolecular CH/π and C–H/O interactions determines whether the spontaneous physisorption of **PF8** at the (110) surface occurs in the presence of a solvent quantity of toluene. Moreover, time-dependent density functional theory (TD-DFT) with Becke three parameter Lee-Yang-Par (B3LYP) method and 6-31 G(d.p) basis set [55–57] calculations of a model fluorene 9-mer indicated that the π–π^* absorption wavelength largely depends on the regularity of the dihedral angles between the fluorene rings, and the intensity and spectral width of the π–π^* absorption band are greatly affected by the regularity of the dihedral angles. This idea is applicable to real **PF8** in solution to determine whether **PF8** spontaneously physisorbs at the (110) and other facets of γ-alumina. Invisible, multiple intermolecular non-covalent bond interactions among the polymers, surface, and solvents are crucial for solution-phase physisorption.

Experimental section and theoretical simulations

Previously, we designed all the procedures for spectroscopic studies of **PF8** physisorption under *quasi-concentrated* solution conditions (1.0×10^{-2} M) in chloroform [44, 45]. In this study, we conducted *dilute/semi-dilute* conditions (1.0×10^{-3} M) of three fractionated **PF8** samples in toluene. Moreover, major difference of the adsorbate is amorphous silica [44] and crystalline γ-alumina in this work.

Detailed experimental and theoretical procedures are described in the Supplementary Information (SI, Figures S1, S2, S4). Herein, **PF8** with $DP_n = 53$ ($PDI = 1.3$), 97 ($PDI = 2.0$), and 200 ($PDI = 2.5$) are abbreviated as **PF8-53**, **PF8-97**, and **PF8-200**, respectively. We confirmed the crystal structure and morphology of neutral γ-alumina [γ-alumina 90, Merck (Tokyo, Japan)] and for comparison, α-alumina [Wako Pure Chemical (Osaka, Japan)], but the number of Al-OH groups on the neutral γ-alumina was unclear and not characterized. A comparison of their scanning electron microscope (SEM) images and wide-angle X-ray diffraction (WAXD) data is given in SI, Figure S3.

Detailed MM/MD simulations with a CVFF force field and quantum mechanical (MP2, density functional theory (DFT), and TD-DFT) calculations are described in the SI. The (110) facet of γ-alumina without OH groups is a built-in inorganic in the Forcite program. In the MM/MD

simulations, we have to consider the effects of AlO–H/**PF8** because O–H/π interactions may exist. Neutral γ-alumina 30 (Merck) is routinely used in column separation experiments due to its certified neutrality (very minimal number of Al–OH groups). Organic chemists often control the surface acidity (the degree of physisorption) of alumina and silica gels by adding methanol, ethanol, and isopropanol to chloroform and hexanes as eluents. The water content of fresh, spectroscopic-grade toluene (Dotite) is less than 0.05% (500 p.p.m.), corresponding to $<0.08 \times 10^{-6}$ mol of water in 3.0 mL of toluene in all the physisorption experiments. Water is not a dominant species compared to 3×10^{-6} mol of the **PF8** repeating unit (10^{-3} M) in 3.0 mL of toluene.

Results and discussion

Physisorption behavior evaluated by UV-visible spectra

Figures 2a–c plots the amount of physisorbed **PF8** with three DP_n (in μmol) onto γ-alumina (0.25 wt/v%) as a function of the physisorption time in toluene at 5, 25, and 50 °C. The initial amounts of γ-alumina, **PF8**, and toluene are 7.5 mg, 1.17 mg, and 3.0 mL, respectively. The nominal ratio of the cross-sectional area of **PF8** to the specific surface area of γ-alumina is ≈4 when the specific surface area of γ-alumina and the cross-sectional area of **PF8** on a flat surface [44, 45] are assumed to be $105 \, m^2 \, g^{-1}$ and 1.33–$1.55 \, nm^2$, respectively, regardless of the face-on, edge-on, and face-on orientations [44] of **PF8**.

Among the three **PF8**, **PF8-97** obviously adsorbed onto γ-alumina at 5, 25, and 50 °C in the adsorption time. However, **PF8-53** scarcely adsorbed onto γ-alumina at these temperatures, and the amount of physisorption diminished by 3-orders of magnitude. Physisorption of **PF8-200** was not clearly detected by UV-visible absorption measurements. Only highly sensitive photoluminescence (PL) and PL excitation (PLE) measurements detected physisorbed **PF8-200** on γ-alumina. Therefore, we can discuss the physisorption behavior associated with the β-phase fraction of non-charged **PF8** on the neutral surface of γ-alumina by the analyses of PL, PLE, and UV-visible absorption spectral data sets as functions of the DP_n, l_K, and q values.

Figure 3a plots the amount of physisorbed **PF8** on γ-alumina (0.25 wt/v%) in toluene as a function of DP_n at 5, 25, and 50 °C for a fixed physisorption time of 3 h. **PF8** almost linearly adsorbed onto γ-alumina at 25 °C for 3 h of physisorption time as DP_n increased. The amount of physisorbed **PF8-200** reached 0.55 μmol per 7.5 mg of γ-alumina ($0.79 \, m^2$) in toluene (0.25 wt/v%) as a function of DP_n at 5, 25, and 50 °C for a physisorption time of 3 h,
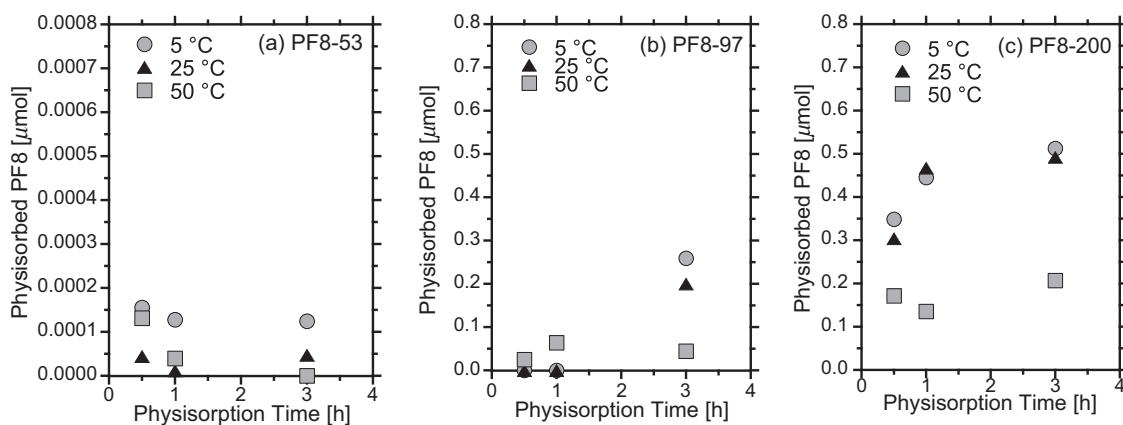
Fig. 2 The amount (in µmol) of physisorbed (**a**) **PF8-53**, (**b**) **PF8-97**, and (**c**) **PF8-200** on γ-alumina (0.25 wt/v%) in toluene at three physisorption temperatures (5, 25, and 50 °C) as a function of the physisorption time

Fig. 3 a The amount (in µmol) of physisorbed **PF8** on γ-alumina (0.25 wt/v%) in toluene as a function of DP_n at 5, 25, and 50 °C for a fixed 3 h physisorption time. **b** Change in the attractive energy between 9,9-di-n-octylfluorene (**F8**) and the (110) surface of γ-alumina as a function of the repeating number (*DP*) of **F8**
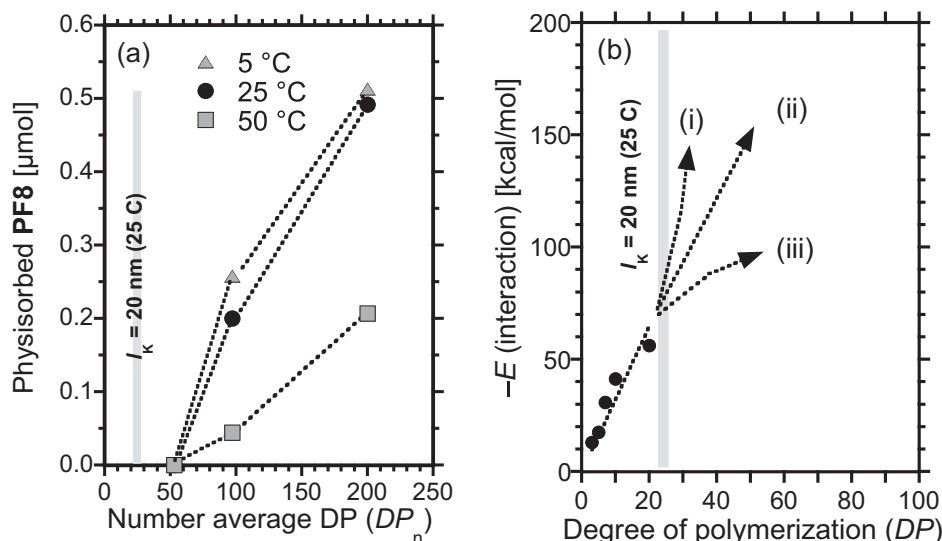
corresponding to ≈60% coverage of **PF8** on the surface. **PF8-97** had a tendency to strongly adsorb when the temperature decreased from 50 °C to 25 °C and 5 °C. However, **PF8-53** weakly adsorbed onto γ-alumina, and the adsorption was independent of the temperature.

At 5 °C and 50 °C, **PF8-200** scarcely adsorbed due to undetermined reasons. An optimal DP_n of **PF8** for physisorption on γ-alumina may exist. We assume that a greater flexibility of the main-/side-chains, as well as the surrounding solvent molecules at elevated temperature may lead to diminish London dispersion and other weak attractive interactions among **PF8**, toluene and the γ-alumina surface.

The q value of **PF8** is 9.8 nm at 25 °C and 33.5 nm at 50 °C in toluene [37] and 8.5 nm in chloroform at 25 °C [33], yielding a Kuhn length ($l_K = 2 \times q$) of 20 nm at 25 °C, 67 nm at 50 °C (in toluene), and 17 nm at 25 °C (in

chloroform). The l_K values in toluene correspond to $DP \approx 25$ at 25 °C and ≈84 at 50 °C when the length of the fluorene monomer unit is assumed to be ≈0.80 nm. The Hildebrand and Hansen solubility parameters [58, 59] indicated that chloroform and toluene act as good and moderate solvents for **PF8**, respectively [33]. Other polyfluorenes carrying chiral alkyl side chains have a similar q value of 9.5 nm in tetrahydrofuran at 20 °C [60].

To discuss the physisorption behavior of **PF8** on a γ-alumina surface as a function of DP_n, we employed MM and MD simulations to evaluate the attractive energy ($-E$, kcal mol^{-1}) between an isolated 9,9-di-n-octylfluorene (**F8**) oligomer (repeating number (*DP*): 3, 5, 7, 10, and 20) and the (110) surface of γ-alumina in a vacuum in association with the q value of **PF8**. Here, interchain interactions among multiple **F8** oligomers were ignored in this simulation. Representative snapshots (0.0, 0.12, 0.25, and 0.50 ns) of spontaneous
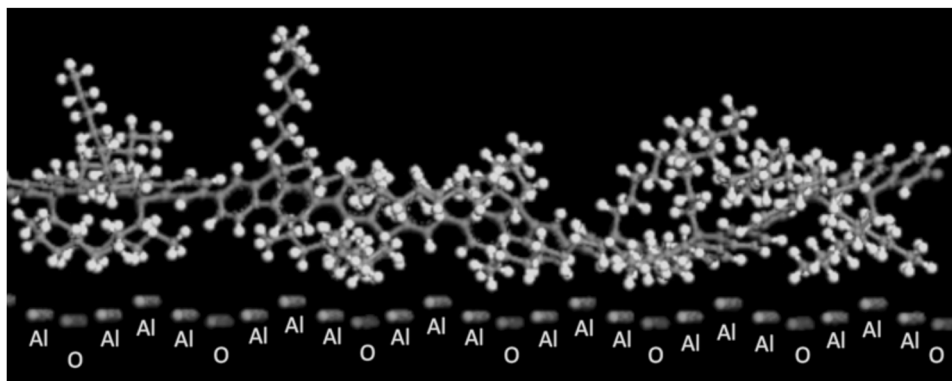
Fig. 4 Magnified snapshot ($t = 0.50$ ns) obtained with an MM/MD simulation of **F8-20** on the (110) surface of γ-alumina in a vacuum at 300 K. A Forcite module with a consistent valence force field (CVFF) in Materials Studio (ver.7, BIOVIA, San Diego, CA, US) was used. Al and O elements are given with labels for visibility

physisorption behaviors of **F8** with $DP = 20$ (**F8-20**) are given in Fig. 4, the SI, Figure S9, and the corresponding movie, DPn20re_on_surf Quench_300K_end_s.mov. For comparison, the physisorption behaviors of **F8-20** are given in DPn20re_278K.mov in the SI. Interestingly, **F8-20** at 5 °C does not adhere well at the surface and tends to form a coiled or looped shape at the surface.

As given in Fig. 3b, the $-E$ value tends to almost linearly increase with an increase of DP up to 20, which nearly corresponds to the l_K value of 20 nm of **PF8** in toluene at 25 °C. An open question is whether the $-E$ value non-linearly increases (case i), increases linearly (case ii), or saturates at a constant value (case iii) when DP_n ranges from 20 and 200. However, we cannot obtain the $-E$ value when DP is sufficiently high due to the limited computing cost for MD simulations. Actually, the simulation took 53 h using our 8-core server for **PF8** with $DP = 20$ in a vacuum (SI, Figures S10 and S11). Nevertheless, Fig. 3a implies experimentally that **PF8** in toluene at 25 °C tends to almost linearly adsorb onto the γ-alumina surface as a function of DP_n. The amounts of physisorbed **PF8** at lower temperatures (5 °C and 25 °C) are larger than those at 50 °C, suggesting that **PF8** desorbs from the surface due to solvation by toluene molecules. Indeed, a noticeable DP dependency of an ordered β-phase formation in a series of 9,9-di-*n*-octylfluorene oligomers was reported[61].

Fraction of β-phase PF8 on γ-alumina surface by PLE and PL spectra

To spectroscopically evaluate the mole fraction of β-phase on the surface of γ-alumina, PL and PLE spectra were taken for **PF8-53**, **PF8-97**, and **PF8-200** adsorbed on γ-alumina. The existence of the β-phase [33–40, 44] indicates a helically well-ordered 5/2 conformation of fluorene with a left-helix or right-helix. Disregarding the physisorbed amount of

PF8, we summarized the normalized PLE and PL spectra in Fig. 5a–f.

The polymer was excited at 360 nm for the PL study, while the spectra were monitored at 480 nm for the PLE study. Each spectrum was normalized at its maximum intensity. Physisorption conditions were γ-alumina (0.25 wt/v%) in toluene at 5, 25, and 50 °C for a physisorption time of 3 h. A comparison of Fig. 5a–c shows that **PF8-97** and **PF8-200** clearly have an intense, narrow PLE (0-0) band at 433 nm, which is characteristic of the β-phase. However, **PF8-53** did not show the 433-nm PLE band and showed a broader vibronic PLE band at ≈375 nm with several shoulder signals. The 433-nm PLE intensity of **PF8-97** tended to increase as the physisorption temperature decreased.

Meanwhile, the 433-nm PLE intensity of **PF8-200** tended to increase as the physisorption temperature decreased. Figures 5e and f show that **PF8-97** and **PF8-200** have four sharp regression PL bands at 438 nm (0–0), 460 nm (0–1), 499 nm (0–2), and ≈534 nm (0–3). The Stokes' shift between the 438 nm (0–0) band and 433 nm PLE (0–0) band is only 5 nm, corresponding to 265 cm^{-1}. The energy spacings between the four PL regressions are 1090, 1700, and 1320 cm^{-1}, respectively. These PL characteristics arise from the well-ordered β-phase. The fraction of the β-phase for **PF8-97** at 25 °C and **PF8-200** at 25 °C was spectroscopically evaluated to be 22 and 29%, respectively. These β-phase fractions are almost half of that (51–56%) for **PF8** on spherical, amorphous silica under quasi-concentrated conditions [44, 45]. The higher fraction of the β-phase in the *dilute/semi-dilute* conditions possibly occurs due to solution-phase epitaxy growth at the crystalline surface.

However, Fig. 5d shows that **PF8-53** has three broad regression PL signals at short wavelengths of 421 nm (0–0), 442 nm (0–1), and ≈508 nm (0–2). The large Stokes' shift between the 421 nm (0–0) and 375 nm PLE (0-0) bands is
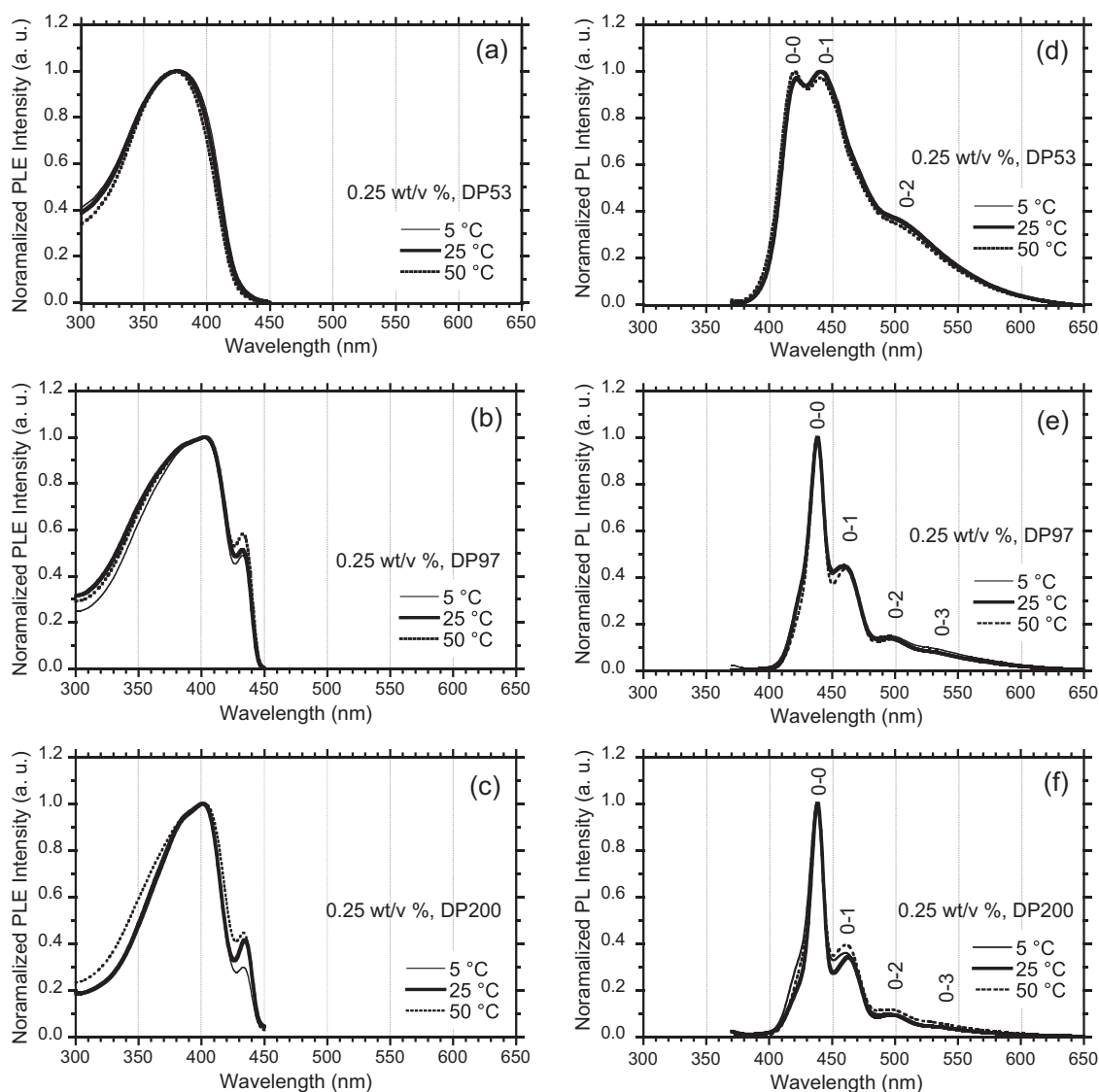
Fig. 5 Photoluminescence excitation (PLE) spectra monitored at 480 nm of (**a**) **PF8-53**, (**b**) **PF8-97**, and (**c**) **PF8-200** on γ-alumina and the corresponding photoluminescence (PL) spectra excited at 360 nm of

(**d**) **PF8-53**, (**e**) **PF8-97**, and (**f**) **PF8-200**. Physisorption conditions are γ-alumina (0.25 wt/v%) in toluene at 5, 25, and 50 °C for a 3 h physisorption time

≈46 nm, corresponding to 2910 cm^{-1}. The energy spacings between the three regression PLs are 1130 and 2940 cm^{-1}, respectively. These PL characteristics arise from the α-phase and other ill-ordered phases. Very similar DP_n-dependent PLE and PL characteristics for 0.50 wt/v% and 1.00 wt/v% of γ-alumina were found at three temperatures (SI, Figures S5–S6).

MM/MD simulations of 9,9-di-*n*-octylfluorene (F8) oligomers onto the (110) surface of γ-alumina in a vacuum and in toluene

A previous section showed that the **F8** oligomer at the (110) surface in a vacuum had a tendency to almost linearly adsorb

with an increase in the *DP* value. The value of –*E* is estimated to be ≈2.5 kcal per **F8** repeating unit-mol. If the –*E* value is extended to $DP = 50$ and 100, the –*E* values reach 125 and 250 kcal per **F8** unit-mol, respectively. These negative value energies are equal to ≈1.4 times and ≈2.8 times, respectively, the bond dissociation energy (89 kcal mol^{-1}) of the C–C single bonds. Actually, the physisorption of **PF8** abruptly occurs between $DP_n = 50$ and 100 (Fig. 3a). A threshold *E* value for efficient spontaneous physisorption in the absence of less-polar toluene, which is similar to the vacuum condition, may exist between ≈150 and ≈300 kcal per mol.

Recently, Katrusiak et al. showed the existence of intermolecular CH/π and CH/HC interactions among toluene molecules in pressured crystals and aggregate forms

[62]. This knowledge prompted us to survey the intermolecular CH/π, π/π, and other possible interactions among toluene, **PF8**, and the (110) surface of γ-alumina as a function of time with the help of MM/MD simulations. To generate a more realistic physisorption model, we set up a hybridized system of one hypothetical **F8** molecule with $DP = 5$ (**F8-5**) (7.8% by volume) at the (110) surface surrounded by 200 hypothetical toluene molecules (92.2% by volume) using an amorphous cell with the Forcite geometry optimization algorithm. The $DP = 5$ and including a number of toluene molecules required substantial computing resources (≈46 h with 8 cores); thus, our computational simulation was limited to $N = 5$ in that environment (SI, Figures S10 and S11).

Figures 6a-f displays the magnified snapshots of the non-adsorbed ($t = 0.0$ ns) and adsorbed ($t = 0.50$ ns) states for **F8-5** onto the (110) surface of γ-alumina at 300 K obtained with the MM/MD simulations associated with the corresponding original movie in SI, pentamer_g-al2O3-11.mov.

When $t = 0.0$ ns, the aromatic C–H protons of toluene interact with the CH_2 protons of the n-octyl groups in **F8-5** via multiple CH/π interactions [49–51], as shown in Figs. 6a–b. The multiple CH/O interactions between aromatic C–H on toluene and O-Al on the (110) surface can be seen in Fig. 6c.

When $t = 0.5$ ns, the CH_2 protons of the n-octyl groups in **F8-5** interact well with O-Al at the (110) surface (Figs. 6d-f), while the aromatic C–H protons of toluene with O–Al at the (110) surface via multiple CH/O interactions [53, 54], as shown in Fig. 6d.

Based on the MM/MD simulations of **F8-5** in toluene, we assume that the origin of spontaneous physisorption of **PF8-97** and **PF8-200** in toluene may be a process of replacing weaker intermolecular CH/π interactions [49–51] existing between the n-octyl chains (C–H) of **PF8** and π-carbons of toluene with stronger intermolecular CH/O interactions [52–54] between n-octyl chains (C–H) and O–Al at the (110) surface. Actually, CH/π and CH/O interactions are ≈1.5 and ≈2.0 kcal mol^{-1}, respectively. The intermolecular CH/O interactions between the aromatic CH of toluene and O-Al at the (110) surface commonly coexist during the spontaneous physisorption of **PF8**.

The adsorbed **PF8** at the γ-alumina (110) can adopt three orientations (face-on, edge-on, and end-on), which is similar to spherical silica [44, 45]. The MM/MD simulations tell us that **PF8** prefers the face-on/edge-on orientations, and while the fluorene main chains are not coplanar, they are not ill-ordered. Non-directional interactions between the n-octyl side chains and the (110) surface are responsible for the ill-ordered main-chain geometry due to non-directional, but stronger intermolecular CH/O interactions [49–54].

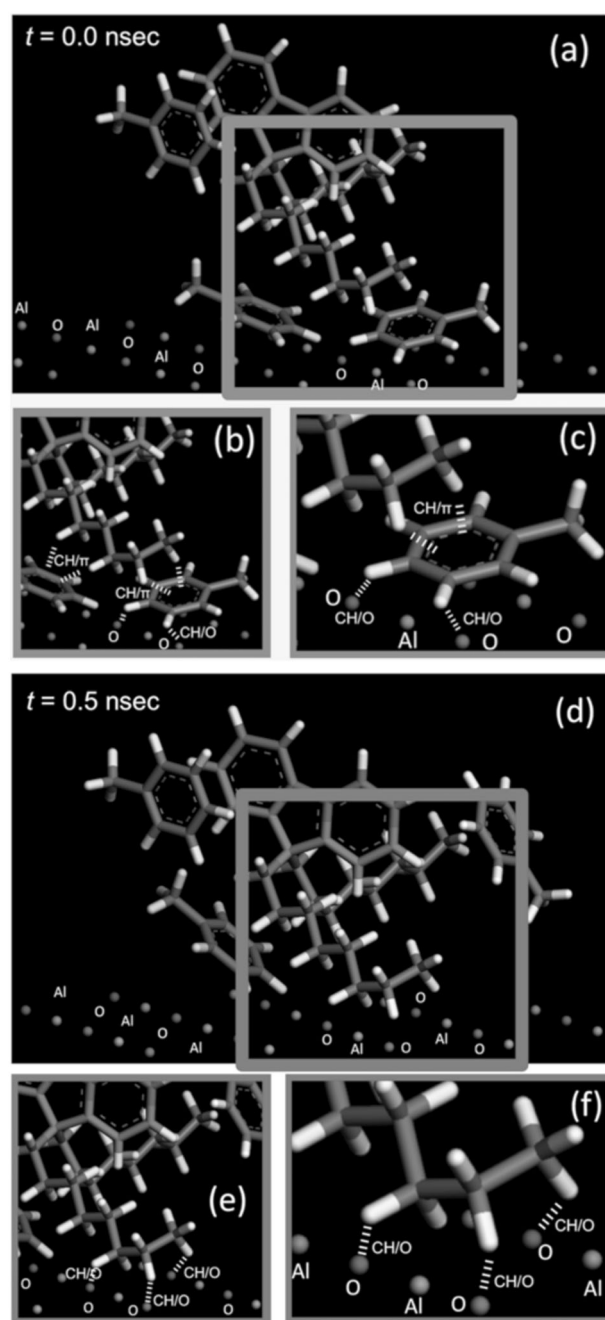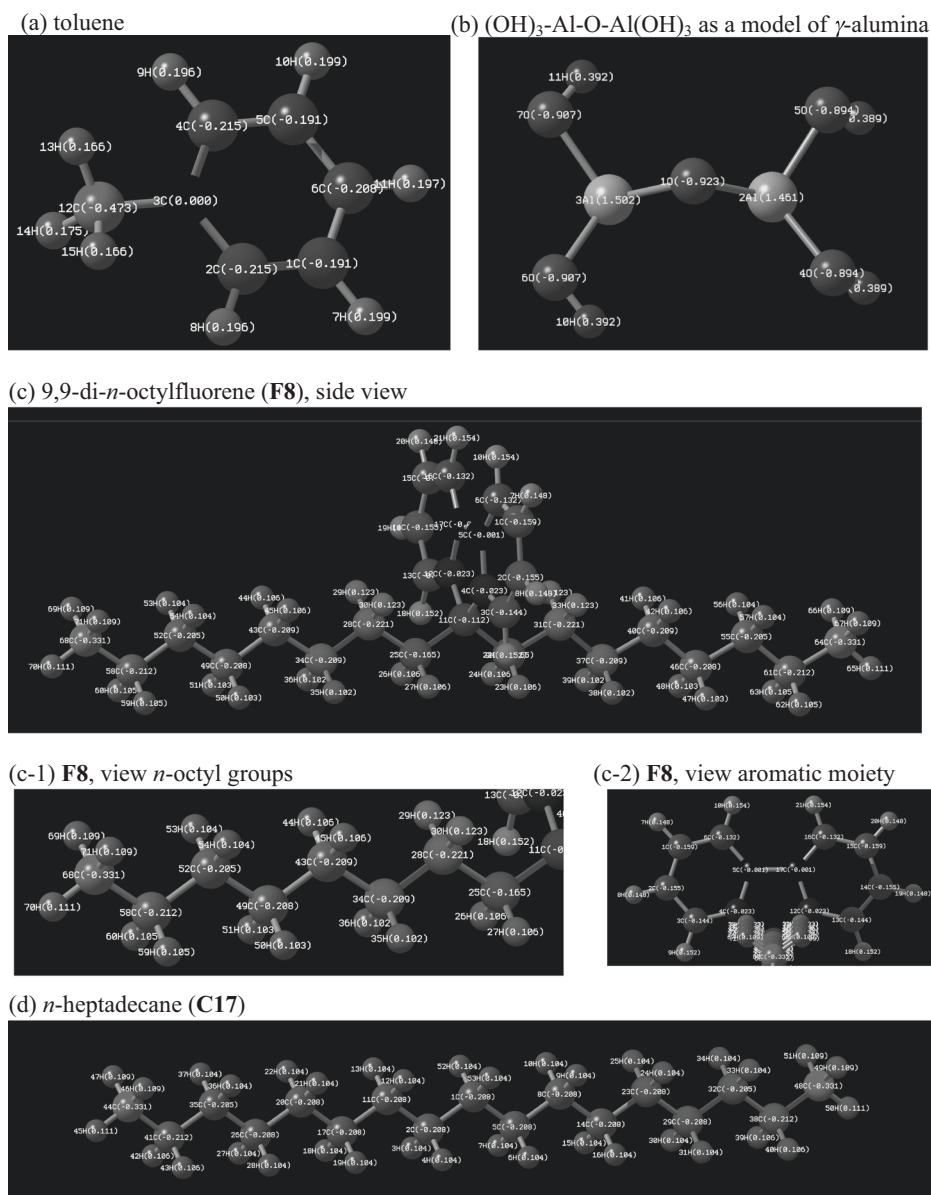To prove the idea, we compared the Mulliken charges between **F8**, toluene, n-heptadecane (**C17**), and a dimeric

Fig. 6 The magnified snapshots of non-adsorbed ($t = 0.0$ ns) and adsorbed ($t = 0.50$ ns) states for **F8** with $DP = 5$ (**F8-5**) on the (110) surface of γ-alumina at 300 K in the presence of a solvent quantity of toluene obtained with MM/MD simulations. When $t = 0.0$ ns, the coexistence of multiple CH/π interactions between the aromatic C–H of toluene and the CH_2 protons of the n-octyl groups in **F8-5** and (Figs. 6a, 6b) multiple CH/O interactions between the aromatic C–H of toluene and O–Al on the (110) surface (Fig. 6c) can be seen. When $t = 0.5$ ns, the multiple CH/O interactions between the CH_2 protons of the n-octyl groups in **F8-5** and O–Al at the (110) surface can be seen (Figs. 6d, 6e, 6f). The Forcite module (CVFF) was used. Al and O elements are given with labels for visibility

Fig. 7 Mulliken charges of (**a**) toluene, (**b**) a dimeric Al-O model of alumina, (**c**) **F8**, and (**d**) *n*-heptadecane (**C17**) obtained with MP2 (6-31 G(d,p) basis set) calculations, in which all geometries were optimized by PM6, DFT (6-31 G(d,p)), and MP2 (6-31 G(d,p))

(a) toluene

(b) (OH)$_3$-Al-O-Al(OH)$_3$ as a model of γ-alumina

(c) 9,9-di-*n*-octylfluorene (**F8**), side view

(c-1) **F8**, view *n*-octyl groups

(c-2) **F8**, view aromatic moiety

(d) *n*-heptadecane (**C17**)

Al-O model of alumina that were obtained with MP2 (6-31 G(d,p) basis set) calculations (Fig. 7) [47, 48], in which all the geometries were optimized by PM6, followed by density functional theory (DFT) with B3LYP method and 6-31 G(d, p) basis set.

It is obvious that the Mulliken charges of hydrogen connected to the aromatic carbons of both toluene and **F8** were commonly $\delta+$, ranging from $+0.196$ and $+0.199$ for toluene and from $+0.148$ and $+0.154$ for **F8** (Fig. 7a, c, 7c-2). Similarly, the Mulliken charges of the C-H protons on the *n*-octyl chains of **F8** were commonly δ^+, ranging from $+0.104$ and $+0.111$ (Fig. 7c, 7c-1). Additionally, the C-H protons on the *n*-alkyl chains of **C17** were commonly δ^+, ranging from $+0.104$ (CH$_2$) and $+0.111$ (CH$_3$) (Fig. 7c-1). Note that the Mulliken charge of H at the β-CH$_2$ in the *n*-octyl chains of **F8** has a somewhat large positive value of $+0.123$ compared to that of the other CH$_2$ groups (Fig. 7d). The β-CH$_2$ with a more positive charge may be responsible for the intramolecular C-H/π interactions [42, 43]. Although the H($\delta \approx +0.4$)-O($\delta \approx -0.9$) group at the γ-alumina was ignored in this calculation (Fig. 7b), an attractive intermolecular AlO-H/π (fluorene ring) interaction should contribute to the spontaneous physisorption.

On the other hand, the aromatic carbons (1 C, 2 C, 4 C, 5 C, and 6 C) of toluene and the aromatic carbons (1 C, 2 C, 3 C, 6 C, 13 C, 14 C, 15 C, and 16 C) of **F8** were commonly δ^-, ranging from –0.191 and –0.215 for toluene and from –0.132 and –0.159 for **F8** (Fig. 7c, 7c-2). The Mulliken charges of O–Al in the dimeric model of γ-alumina were largely a minus charge of $\delta = -0.923$ (Fig. 7b).

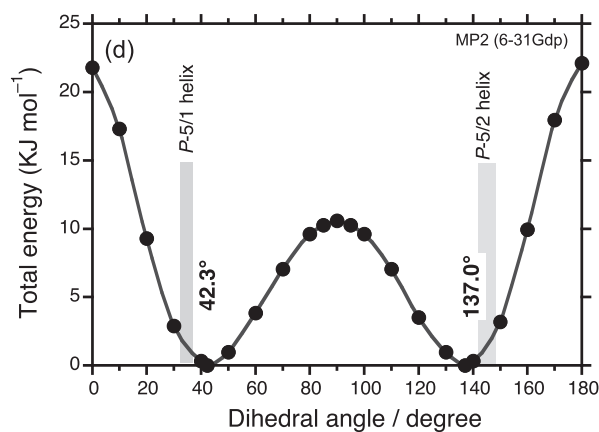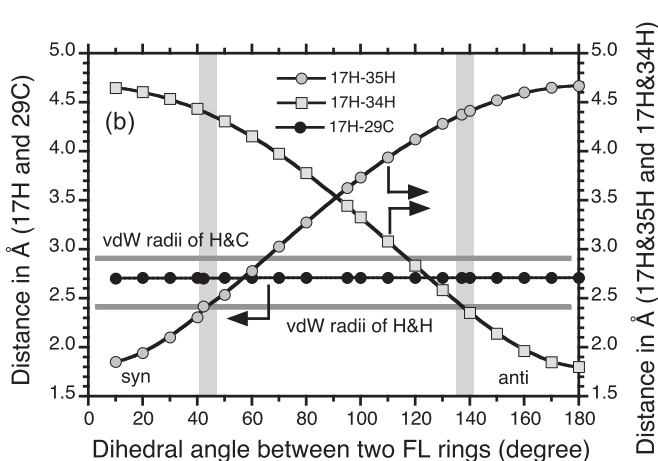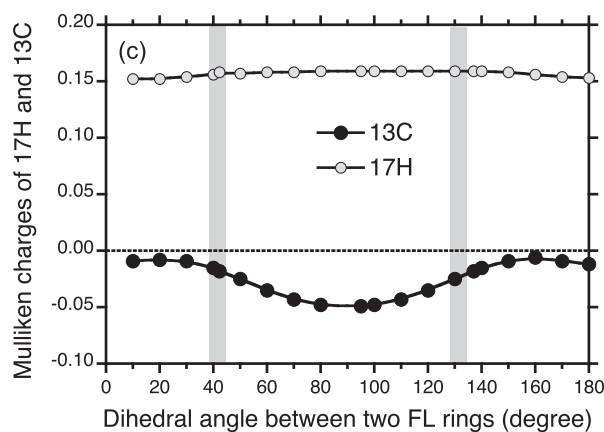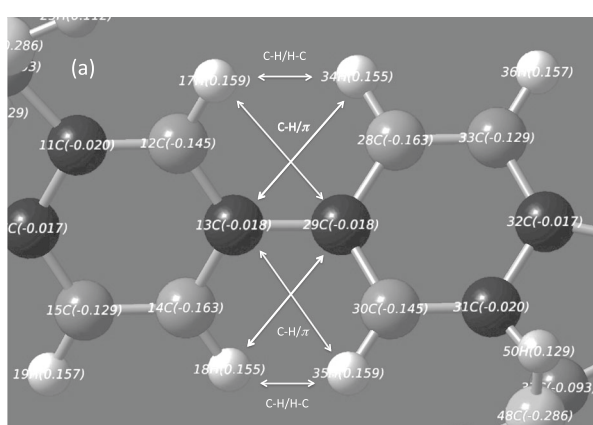**Fig. 8 a** Mulliken charges of **F1-2** obtained with MP2 (6-31 G(d,p) basis set) calculations, in which all geometries were optimized by PM6, DFT (6-31 G(d,p)), and MP2 (6-31 G(d,p)). **b** Distance between 17 H and 29 C as a function of the dihedral angle of the **F1-2** rings. **c** Mulliken charges between 17 H and 29 C as a function of the dihedral angle of the **F1-2** rings. **d** Potential energy of the 9,9-dimethylfluorene 9-mers (**F1-9**) as a function of the dihedral angle of the **F1-2** fluorene rings

Intramolecular attractive CH/π and CH/O interactions were normally weak [49–54] but can be greatly boosted by multiple interactions between *H* and *C/O* elements due to a linear amplification scenario with an increase of the *DP* value.

More positive Mulliken charges and multiple C–*H* interactions with the solvent quantity of toluene are likely to more strongly interact with the γ-alumina surface compared to **F8** and smaller *DP* values of **PF8**. Thus, the alkyl chains and aromatic carbons of **F8** and **PF8** should competitively adsorb to the δ^- charged surface of γ-alumina. To spontaneously adsorb **PF8** molecules onto the γ-alumina surface, a critical *DP* value of **PF8** may exist to exceed the multiple CH/O interactions existing between toluene and *O*–Al on γ-alumina.

Intramolecular CH/π interactions of 9,9-dimethylfluorene dimer (F1-2) as a model of PF8

Our previous work on aggregation-induced emission experiments of **PF8** in a solvent quantity of *D-/L*-limonene indicated that the β-phase at ≈430 nm may exist as an enantiomeric mixture of *left*-handed and *right*-handed helical motifs [63]. Higher order structures, including the appearance of the β-phase of **PF8**, are susceptible to molecular weight, the nature of solvents (good or poor), temperature, and annealing processes. Previously, we ascribed the highly emissive characteristics of **PF8** in the solid state to the intramolecular CH/π interactions between the H at the β position of the *n*-octyl groups and the *ipso*-carbons of the fluorene rings in **PF8** (Fig. 1, top right), leading to an avoidance of ACQ of the π-luminophores[42].

Herein, we propose additional intramolecular CH/π interactions between the *H* in the aromatic carbons and the *ipso*-carbons in **PF8**, leading to spontaneous twisting in the *left*-handed or *right*-handed fluorene main chains (Fig. 8a). The opposite Mulliken charges between the *H*–π ring and C_{ipso}–π ring of **F1-2** may cause a short distance of ≈2.70 Å between the *H*–π and C_{ipso}–π rings, while van der Waals contacts between *H* and π are 2.90 Å and 2.84 Å, as provided by Bondi [64] and Rowland–Tayler [65],
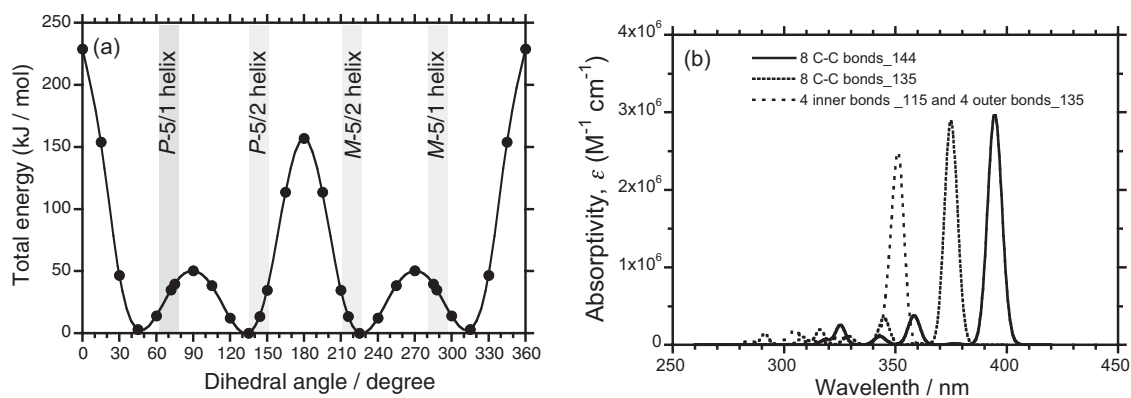
Fig. 9 **a** Total energy of the 9,9-dimethylfluorene 9-mer (**F1-9**) obtained with DFT (B3LYP, 6-31 G basis set) optimized by PM6. **b** UV-visible absorption spectra of **F1-9** with a hypothetical β-phase (dihedral angle of 144°, bold solid line), global minimum (dihedral angle of 135°, dotted line), and hypothetical disordered conformation consisting of two dihedral angle sets (115° and 138°) between the fluorene rings (broken line). All FWHMs are fixed at 0.03 eV

respectively (Fig. 8b and the SI, Figure S12). This intramolecular CH/π interaction within multiple fluorene rings is assumed to be an another determining factor in causing a structural transition from a thermodynamically metastable, ill-ordered to a thermodynamically stable, well-ordered conformation like the β-phase upon thermal annealing and/or exposure to solvent vapor.

The MP2 calculations suggested the existence of intramolecular CH/π interactions between the four *H* (17 H, 34 H, 18 H, and 35 H) with positive charges, ranging from $\delta \approx + 0.155$ and $+0.159$, on the fluorene ring carbon and four *ipso-carbons* (13 C and 29 C) with a weak negative charge of $\delta = -0.018$ on the rings, leading to a shorter C–H/π distance of ≈ 2.70 Å (Fig. 8c, SI, Figure S12). This distance can be compared to van der Waals contact between H and C of 2.84–2.90 Å. Meantime, the distances between 17 H and 34 H and between 18 H and 35 H are maintained at their van der Waals contact of 2.40 Å[64] (Fig. 8b).

F1-2 has two local minima at dihedral angles of 42.4° (*syn-form*) and 137.0° (*anti-form*). These dihedral angles are close to the 5_1 and 5_2 helices of **PF8** with *P*-screw-sense (Fig. 8d). The origin of the local minima can be ascribed to a balance of the intramolecular attractive CH/π and repulsive H/H interactions among the four *H* and four *ipso-carbons*.

Multiple CH/O interactions between the positively charged *H* and the negatively charged *O* elements at the (110) surface can coexist. These multiple, weak intramolecular CH/π, H/H, and intermolecular CH/O interactions may be the factors that determine whether the **PF8** main chain can adopt the ordered β-phase or disordered phases at the surface. As a result, the fraction of β-phase is susceptible to the solution temperature, surface state, DP_n, and nature of solvents.

Effects of the regularity and irregularity of the main chain dihedral angles affecting the π–π* main chain absorption characteristics of 9,9-dimethylfluorene 9-mer (F1-9) as a model of PF8

We investigated the effects of the regularity and irregularity of the main chain dihedral angles that can modulate the π–π* main chain absorption characteristics of **PF8** using its oligomer model of 9,9-dimethylfluorene 9-mer (**F1-9**) and the TD-DFT (6-31 G(d.p) basis set, 20 singlet states) by optimizing **F1-9** at $\approx 135°$ with DFT (6-31 G(d.p) basis set).

Similar to **F1-2**, **F1-9** has four local minima at dihedral angles of 45° (*P-syn*), 135° (*P-anti*), 235° (*M-syn*), and 315° (*M-anti*) in a vacuum (Fig. 9a). The angles of 45° and 315° are close to the 5_1 helix with a dihedral angle of 36° or 324°, while the angles of 135° and 215° are close to the 5_2 helix (dihedral angles of 144° and 216°).

F1-9 compares the π-π* absorption spectra of three hypothetical **F1-9** models with a fixed full-width-at-the-half maximum (FWHM) of 0.03 eV (Fig. 9b), including a hypothetical, but not global minimum conformation in the β-phase (dihedral angle of 144°, solid line), a global minimum (dihedral angle of 135°, dotted line), and a hypothetical, disordered conformation consisting of two dihedral angle sets (115° and 138°) in the fluorene rings (broken line).

Clearly, **F1-9** with a constant dihedral angle of 144° shows the longest π–π* absorption band at 394 nm among the three models, while **F1-9** with a constant dihedral angle of 135° at the local minimum has a shorter π–π* absorption at 374 nm. However, their absorptivity (ε) values are nearly the same, i.e., $\approx 2.9 \times 10^6$ M^{-1} cm^{-1}. On the other hand, **F1-9** with two dihedral angle sets of 115° (inner four C–C bonds) and 138° (outer four C–C bonds) has the shortest π-π* band at 351 nm, which is associated with a broader, weaker band intensity of $\varepsilon = 2.5 \times 10^6$ M^{-1} cm^{-1}.
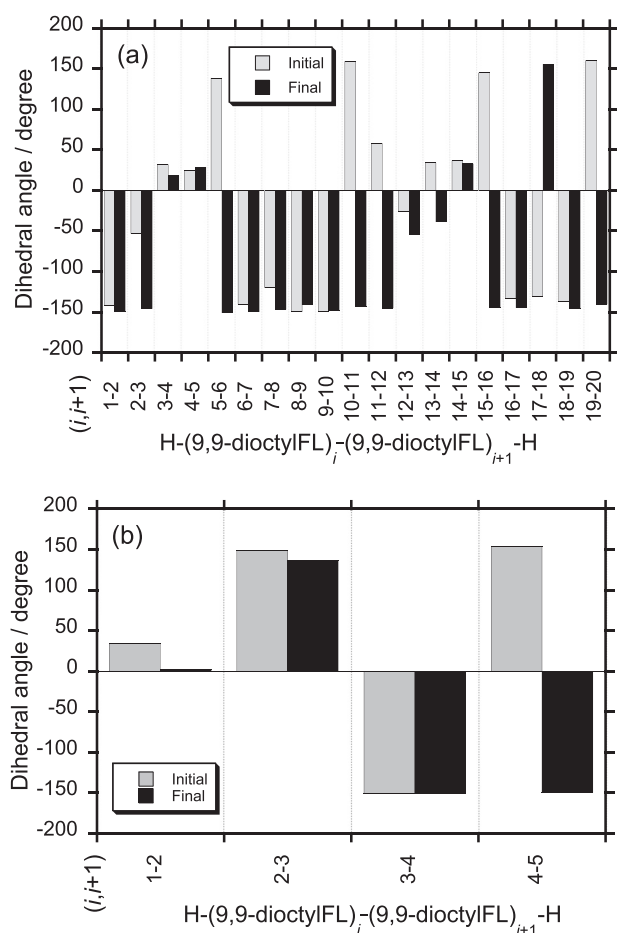
Fig. 10 a The distributions in the dihedral angle sets of (a) F8-20 in a vacuum and (b) F8-5 in toluene before physisorption (gray solid bars, $t = 0.0$ ns for F8-20 and F8-5) and after physisorption (black solid bars, $t = 1.0$ ns for F8-20 and 0.5 ns for F8-5) obtained with MM/MD calculations (Figs. 5, 6, S9, and S11)

These simulations of F1-9 predict that the π-π* absorption band wavelength (λ_{max}) largely depends on the regularity of the dihedral angles, while the π–π* absorption band intensity (ε) and spectral width are significantly affected by the regularity of the dihedral angles. This idea is applicable to a real PF8 system when PF8 physisorbs at the (110) surface of γ-alumina and amorphous silica.

Moreover, the MM/MD calculations taken from Figs. 5, 6, S9, and S11 and a data analysis of their dihedral angle sets indicate that before physisorption in a vacuum, F8-20 initially adopts a randomly twisted irregular main chain geometry with a shorter M-sense sequence, e.g., $(i, i + 1) =$ 5–6, 7–8, 8–9, 9–10, and $(i, i + 1) =$ 16–17, 17–18 (Fig. 10a, gray bar). After physisorption on the (110) of alumina, F8-20 changes into a longer, regular M-sense sequence with the dihedral angle $\approx -150°$ (Fig. 10a, black solid bar), e.g., $(i, i + 1) =$ 5–6 to 11–12 by changing the dihedral angles from $+130°$ at $(i, i + 1) =$ 5–6, $+150°$ at $(i, i + 1) =$ 10–11, $-25°$ at $(i, i + 1) =$ 12–13, and $+20°$ at $(i, i$

$+ 1) = 13$–14. This tendency predicts that a spontaneous propagation of the β-phase-like structure for the longer F8-20 is likely to occur at the (110) surface. However, this tendency is not obvious for the shorter F8-5 in toluene (Fig. 10b, black and gray solid bars). A sufficiently longer PF8 chain may help to initially generate a short β-like sequence, which is followed by propagation to a regular β-phase upon physisorption at the γ-alumina. This idea could provide a possible explanation for our observation at the polymer–polymer interface, in which an optically active, rigid, rodlike, Si–Si bond polymers with one or two monolayers at the surface can efficiently transfer their preferable helicity to a non-helical, semiflexible, Si-Si bond polymer as a thick film, providing greatly enhanced circular dichroism signals [68].

Summary and outlook

We spectroscopically investigated how non-charged, semiflexible PF8 spontaneously physisorb onto the neutral surface of cuboidal γ-alumina (specific surface area ≈90–120 $m^2 g^{-1}$) in toluene at 5, 25, and 50 °C. PF8 with three different DP_n with a narrower PDI was used for the photoluminescent adsorbate. PF8 revealed noticeable DP_n and temperature dependencies of its physisorption behaviors based on the analysis of the experimental data sets.

MM/MD simulations (CVFF force field) and MP2 (6-31 G(d,p) basis set) calculations led us to propose a physisorption scenario for PF8 at the γ-alumina surface in toluene; i.e., a swap from multiple CH/π interactions between PF8 and toluene to multiple C–H/O interactions between PF8 and γ-alumina is occurring. The competition between multiple intramolecular CH/π and intermolecular C-H/O interactions among PF8, toluene, and γ-alumina may be crucial in whether the spontaneous physisorption of PF8 occurs.

The Mulliken charges with the MP2 (6-31 G(d,p) basis set) calculations further suggested intramolecular CH/π interactions between the C-H protons at the fluorene ring and the *ipso-carbons* of the rings because of a shorter C–H/π distance of ≈2.70 Å, which was reflected in the opposite Mulliken charges between the H and C_{ipso} elements. DFT and TD-DFT (B3LYP/6-31 G(d.p)) calculations of the 9,9-dimethylfluorene 9-mer indicated that the π–π* absorption wavelength largely depends on the regularity of the dihedral angles between the nine fluorene rings, while the intensity and spectral width of the π–π* absorption band are greatly affected by the regularity of the dihedral angles. This idea is applicable to the prediction of whether PF8 and other semiflexible polymers spontaneously physisorb at the γ-alumina and other impenetrable surfaces in several proper solvents. The coexistence of intermolecular CH/π and CH/O

interactions between the *n*-octyl groups of **PF8** and cellulose derivatives at heterogeneous polymer–polymer interfaces have been recently reported by us [66, 67]. The present knowledge should be applicable to solution phase-driven physisorption at liquid-solid interfaces and solution phase-driven heterogeneous polymer-polymer interfaces by considering the natures of polymers, surfaces, and solvents.

Compliance with ethical standards

Conflict of interest The authors declare that they have no conflict of interest.

References

1. Parfitt GD, Rochester CH, Editors. Adsorption from solution at the solid/liquid interface. New York: Academic; 1983.
2. Jones RAL, Richards RW. Polymers at surface and interfaces. Cambridge, UK: Cambridge University Press; 1999.
3. Butt H-J, Graf K, Kappl M. Physics and chemistry of interfaces. Germany: Wiley–VCH, Weinheim; 2006.
4. Israelachvili YN. Intermolecular and surface forces. 3rd edn. New York: Academic; 2011.
5. Langmuir I. The adsorption of gases on plane surface. J Am Chem Soc. 1918;40:1361–403.
6. Brunauer S, Emmett PH, Teller E. Adsorption of gases in muiti-molecular layers. J Am Chem Soc. 1938;60:309–19.
7. Simha R, Frish HL, Eirich RR. The adsorption of flexible macromolecules. J Phys Chem. 1953;57:584–9.
8. Dąbrowski A. Adsorption–from theory to practice. Adv Colloid Interface Sci. 2001;93:135–224.
9. Sagiv J. Organized monolayers by adsorption. 1. Formation and structure of oleophobic mixed monolayers on solid surfaces. J Am Chem Soc. 1980;102:92–8.
10. Netzer N, Sagiv J. A new approach to construction of artificial monolayer assemblies. J Am Chem Soc. 1983;105:674–6.
11. Park J-W, Park YJ, Jun C-H. Post-grafting of silica surfaces with pre-functionalized organosilanes: new synthetic equivalents of conventional trialkoxysilanes. Chem Commun. 2011;47:4860–71.
12. Guo G, Naito M, Fujiki M, Saxena A, Okoshi K, Yang Y, Ishikawa M, Hagihara T. Room-temperature one-step immobilization of rod-like helical polymer onto hydrophilic substrates. Chem Commun. 2004;276–7.
13. Yamamoto K, Otsuka H, Takahara A. Preparation of novel polymer hybrids from imogolite nanofiber. Polym J. 2007;39:1–15.
14. Porter MD, Bright TB, Allara DL, Chidsey CED. Spontaneously organized molecular assemblies. 4. Structural characterization of *n*-alkyl thiol monolayers on gold by optical ellipsometry, infrared spectroscopy, and electrochemistry. J Am Chem Soc. 1987;109:3559–73.
15. Berndt P, Kurihara K, Kunitake T. Adsorption of poly(styrenesulfonate) onto an ammonium monolayer on mica: A surface forces study. Langmuir. 1992;113:2486–90.
16. Kumar A, Whiteside GM. Features of gold having micrometer to centimeter dimensions can be formed through a combination of stamping with an elastomeric stamp and an alkanethiol "ink" followed by chemical etching. Appl Phys Lett. 1993;63:2002–4.
17. Lvov Y, Decher G, Möhwald H. Assembly, structural characterization, and thermal behavior of layer-by-layer deposited ultrathin films of poly(vinyl sulfate) and poly(allylamine). Langmuir. 1993;9:481–6.
18. Brust M, Walker M, Bethell D, Schiffrin DJ, Whyman R. Synthesis of thiol-derivatised gold nanoparticles in a two-phase liquid–liquid system. J Chem Soc Chem Commun. 1994;1801–2.
19. Lvov Y, Ariga K, Ichinose I, Kunitake T. Assembly of multicomponent protein films by means of electrostatic layer-by-layer adsorption. J Am Chem Soc. 1995;117:6117–23.
20. Kotov NA, Dekany I, Fendler JH. Layer-by-layer self-assembly of polyelectrolyte–semiconductor nanoparticle composite films. J Phys Chem. 1995;99:13065–9.
21. Decher G. Fuzzy nanoassemblies: toward layered polymeric multicomposites. Science. 1997;277:1232–7.
22. Caruso F. Nanoengineering of inorganic and hybrid hollow spheres by colloidal templating. Science. 1998;282:1111–4.
23. Ejaz M, Yamamoto S, Ohno K, Tsujii Y, Fukuda T. Controlled graft polymerization of methyl methacrylate on silicon substrate by the combined use of the Langmuir-Blodgett and atom transfer radical polymerization techniques. Macromolecules. 1998;31:5934–6.
24. Zhao B, Brittain WJ. Polymer brushes: surface-immobilized macromolecules. Prog Polym Sci. 2000;25:677–710.
25. Matyjaszewski K, Xia J. Atom transfer radical polymerization. Chem Rev. 2001;101:2921–90.
26. Pyun J, Matyjaszewski K. Synthesis of nanocomposite organic/inorganic hybrid materials using controlled "living" radical polymerization. Chem Mater. 2001;13:3436–48.
27. Zhou F, Huck WTS. Surface grafted polymer brushes as ideal building blocks for "smart" surface. Phys Chem Chem Phys. 2006;8:3815–23.
28. Mizukami M, Kurihara K. Macrocluster formation of alcohol on silica surface in cyclohexane: analysis of interfacial energy between adsorption layer and bulk solution. E J Surf Sci Nanotech. 2006;4:244–8.
29. Tsubokawa N. Surface grafting of polymers onto nanoparticles in a solvent-free dry-system and applications of polymer-grafted nanoparticles as novel functional hybrid materials. Polym J. 2007;39:983–1000.
30. Budarin VL, Clark JH, Hale SE, Tavener SJ, Mueller KT, Washton NM. NMR and IR study of fluorobenzene and hexafluorobenzene adsorbed on alumina. Langmuir. 2007;23:5412–8.
31. Pietropaolo A, Wang Y, Nakano T. Predicting the switchable screw sense in fluorene-based polymers. Angew Chem Int Ed. 2015;54:2688–92.
32. Zhang W, Gomez ED, Milner ST. Surface-induced chain alignment of semiflexible polymers. Macromolecules. 2016;49:963–71.
33. Grell M, Bradley DDC, Long X, Chamberlain T, Inbasekaran M, Woo EP, Soliman M. Chain geometry, solution aggregation and enhanced dichroism in the liquid crystalline conjugated polymer poly(9,9-dioctylfluorene). Acta Polym. 1998;49:439–44.
34. Grell M, Bradley DDC, Ungar G, Hill J, Whitehead KS. Interplay of physical structure and photophysics for a liquid crystalline polyfluorene. Macromolecules. 1999;32:5810–7.
35. Scherf U, List EJW. Semiconducting polyfluorenes towards reliable structure-property relationships. Adv Mater. 2002;14:477–87.
36. Knaapila M, Garamus VM, Dias FB, Almásy L, Galbrecht F, Charas A, Morgado J, Burrows HD, Scherf U, Monkman AP. Influence of solvent quality on the self-organization of archetypical hairy rods-branched and linear side chain polyfluorenes: rodlike chains versus "beta-sheets" in solution. Macromolecules. 2006;39:6505–12.

37. Chen J-H, Chang C-S, Chang Y-X, Chen C-Y, Chen H-L, Chen S-A. Gelation and its effect on the photophysical behavior of poly (9,9-dioctlfluorene-2,7-diyl) in toluene. Macromolecules. 2009;42:1306–14.

38. Cone CW, Cheng RR, Makarov DE, V Bout DA. Molecular weight effect on the formation of β-phase poly(9,9-dioctyl-fluorene) in dilute solutions. J Phys Chem B. 2011;115:12380–5.

39. Evans RC, Marr PC. Chain confinement promotes β-phase formation in polyfluorene-based photoluminescent ionogels. Chem Commun. 2012;48:3742–4.

40. Liu C, Wang Q, Tian H, Liu J, Geng Y, Yan D. Morphology and structure of the β-phase crystals of monodisperse polyfluorenes. Macromolecules. 2013;46:3025–30.

41. Mei J, Leung NLC, Kwok RTK, Lam JWY, Tang BZ. Aggregation-induced emission: together we shine, united we soar! Chem Rev. 2015;115:11718–940.

42. Taguchi M, Suzuki N, Fujiki M. Intramolecular CH/π interaction of poly(9,9-dialkylfluorene)s in solutions: Interplay of the fluorene ring and alkyl side chains revealed by 2D ^{1}H-^{1}H NOESY NMR and 1D ^{1}H-NMR experiments. Polym J. 2013;45:1047–57.

43. Suzuki N, Matsuda T, Nagai T, Yamazaki K, Fujiki M. Investigation of the intra-CH/π interaction in dibromo-9,9′-dialkyl-fluorenes. Cryst Growth Des. 2016;16:6593–9.

44. Nakao A, Fujiki M. Visualizing spontaneous physisorption of non-charged π-conjugated polymers onto neutral surfaces of spherical silica in nonpolar solvents. Polym J. 2015;47:434–42.

45. Nakao A. Molecular weight dependency of physisorption behavior. In: Elucidation of physisorption behaviors of π-conjugated polymers and characterization thereof, Chapter 3. PhD thesis, Nara Institute of Science and Technology; 2015, pp 64–96.

46. Bhowmik R, Katti KS, Katti D. Molecular dynamics simulation of hydroxyapatite–polyacrylic acid interfaces. Polym (Guildf). 2007;48:664–74.

47. Møller C, Plesset MS. Note on an approximation treatment for many-electron systems. Phys Rev. 1934;46:618–22.

48. Head-Gordon M, Pople JA, Frisch MJ. MP2 energy evaluation by direct methods. Chem Phys Lett. 1988;153:503–6.

49. Nishio M, Hirota M, Umezawa Y. The CH/π interaction: evidence, nature, and consequences. New York: John Wiley & Sons; 1998.

50. Tsuzuki S, Fujii A. Nature and physical origin of CH/π interaction: significant difference from conventional hydrogen bonds. Phys Chem Chem Phys. 2008;10:2584–94.

51. Takahashi O, Kohno Y, Nishio M. Relevance of weak hydrogen bonds in the conformation of organic compounds and bioconjugates: Evidence from recent experimental data and high-level ab initio MO calculations. Chem Rev. 2010;110:6049–76.

52. Sutor DJ. The CH⋯O hydrogen bond in crystals. Nature. 1962;195:68–9.

53. Desiraju GR. The C–H⋯O hydrogen bond: structural implications and supramolecular design. Acc Chem Res. 1996;29:441–9.

54. Gu Y, Kar T, Scheiner S. Fundamental properties of the CH⋯O interaction: is it a true hydrogen bond? J Am Chem Soc. 1999;121:9411–22.

55. Hohenberg P, Kohn W. Inhomogeneous electron gas. Phys Rev. 1964;136:B864–71.

56. Marques MAL, Ullrich CA, Nogueira F, Rubio A, Burke K, Gross EKU, Editors. Time-dependent density functional theory. Berlin, Germany: Springer-Verlag; 2006.

57. Ullrich C. Time-dependent density-functional theory: concepts and applications. Oxford: Oxford University Press; 2012.

58. Hildebrand JH, Scott RH. The solubility of nonelectrolytes: monograph series. American Chemical Society, No. 17; 2012.

59. Hansen CM. The three dimensional solubility parameter and solvent diffusion coefficient. Copenhagen: Danish Technical Press; 1967.

60. Wu L, Sato T, Tang. H-Z, Fujiki M. Conformation of a poly-fluorene derivative in dolution. Macromolecules. 2004;37:6183–8.

61. Shiraki T, Shindome S, Toshimitsu F, Fujigaya T, Nakashima N. Strong main-chain length-dependence for the β-phase formation of oligofluorenes. Polym Chem. 2015;6:5103–9.

62. Marciniak J, Bakowicz J, Dobrowolski MA, Dziubek KF, Kazmierczak M, Paliwoda D, Rajewski KW, Sobczak S, Stachowicz M, Katrusiak A. Most frequent organic interactions compressed in toluene. Cryst Growth Des. 2016;16:1435–41.

63. Nakano Y, Liu Y, Fujiki M. Ambidextrous circular dichroism and circularly polarised luminescence from poly(9,9-di-n-decylfluorene) by terpene chirality transfer. Polym Chem. 2010;1:460–9.

64. Bondi A. van der Waals volumes and radii. J Phys Chem. 1964;68:441–51.

65. Rowland RS, Taylor R. Intermolecular nonbonded contact distances in organic crystal structures: comparison with distances expected from van der Waals radii. J Phys Chem. 1996;100:7384–91.

66. Guo G, Suzuki N, Fujiki M. Oligo- and polyfluorenes meet cellulose alkyl esters: Retention, inversion, and racemization of circularly polarized luminescence (CPL) and circular dichroism (CD) via intermolecular C-H/O=C interactions. Macromolecules. 2017;50:1778–89.

67. Guo S, Kamite H, Suzuki N, Wang L, Ohkubo A, Fujiki M. Ambidextrous chirality transfer capability from cellulose tris(phenylcarbamate) to nonhelical chainlike luminophores: Achiral solvent-driven helix-helix transition of oligo- and polyfluorenes revealed by sign inversion of circularly polarized luminescence and circular dichroism spectra. Biomacromolecules. 2018;19:449–59.

68. Saxena A, Guo G, Fujiki M, Yang Y, Ohira A, Okoshi K, Naito M. Helical polymer command surface: Thermodriven chiroptical transfer and amplification in binary polysilane film system. Macromolecules. 2004;37:3081–3.